Int. J. Electrochem. Sci., 12 **(2017)** 1306 – 1317, doi: 10.20964/2017.02.28

International Journal of
ELECTROCHEMICAL
SCIENCE
www.electrochemsci.org

Facile Synthesis of Carbon-Encapsulated Fe_3O_4 core/shell Nanospheres for Application in Pb(II) Electrochemical Determination

Shengbo Sang[1], *Hui Zhang*[1,2,*], *Youyi Sun*[3,*], *Aoqun Jian*[1], *Wendong Zhang*[1]

[1] Micro Nano System Research Center, Key Lab of Advanced Transducers and Intelligent Control System of the Ministry of Education &College of Information Engineering, Taiyuan University of Technology, Taiyuan 030024, China.
[2] College of Computer and Control Engineering, North University of China, Taiyuan 030051, China.
[3] Shanxi Province Key Laboratory of Functional Nanocomposites, North University of China, Taiyuan 030051, China.
[*]E-mail: zhanghui_8078@163.com, syyi2010@163.com

Received: 21 October 2016 / *Accepted:* 7 December 2016 / *Published:* 30 December 2016

In this study, carbon-encapsulated Fe_3O_4 core/shell nanospheres (Fe_3O_4@C) were synthesized by a facile method and characterized by transmission electron microscopy, scan electron microscopy, X-ray diffraction , IR spectroscopy and Raman spectroscopy. Furthermore, Fe_3O_4@C nanospheres electrode was characterized by cyclic voltammetry and electrochemical impedance spectra. The Fe_3O_4@C nanospheres electrode exhibited remarkable electrocatalytic activity towards Pb(II) oxidation with higher limit of detection and sensitivity of 0.17μM and 95.6μA/μM compared to other active materials on electrochemical detection of Pb(II) reported in previous works. Moreover, the Fe_3O_4@C nanospheres electrode exhibited high cycling stability and long-term durability. These results were attributed to the porous structure of the Fe_3O_4@C nanospheres electrode, which enabled the Fe_3O_4@C nanospheres to become highly accessible to the metal ion and provided more void volume for the reaction with metal ions. This work suggests that there is great potential in employing the Fe_3O_4@C nanospheres as heavy metal ions sensors.

Keywords: mesoporous carbon, Fe_3O_4, core-shell, electrochemical detection, heavy metal.

1. INTRODUCTION

Heavy metals are the most problematic pollutants as they are non-biodegradable and can accumulate in ecological systems [1]. Especially, copper (Cu), lead (Pb), cadmium (Cd), mercury (Hg) and chromium (Cr) were the most probable causes for most of the heavy metal-related diseases [2-3].

Therefore, sensitive and selective determination of heavy metals was paramount important. There were lot of techniques to be developed for the detection of heavy metal ions, including plasma mass spectrometry energy dispersive X-ray fluorescence (EDXRF), fluorescent spectrometry and electrochemical method [4-6]. Due to the capability of short analytic time, low power cost, and high sensitivity for in-situ measurement [7], electrochemical method has attracted great interest in the detection of heavy metal ions. A key step for electrochemical method to detect heavy metal ions was the design and synthesis of the working electrode materials. The Fe_3O_4 nanoparticles have been widely used in electrochemical sensing due to the characteristics of low-cost, environmentally friendly and easy-preparation [8]. In order to further enhance the sensitivity and reduce the aggregate of Fe_3O_4 nanoparticles, the Fe_3O_4 were generally modified by others materials, such as Au, Ag, graphene, SiO_2, ZrO_2 etc[9-15]. Recently, amorphous carbon have been widely used as suitable modifiers for Fe_3O_4 electrode materials applied in electrochemical energy storage due to be a fast response, a wide dynamic range, reasonable selectivity, an easily renewable surface and low cost[16-17]. In addition to this, the electrode materials with amorphous carbon shell with mesoporous structure was not easily pulverized or broken due to its facile strain relaxation, which could be effective against the volume change problem during electrochemical reaction [18]. Therefore, it was highly desirable to synthesis mesoporous Fe_3O_4@carbon core-shell nanoparticles and further applied in electrochemical detection. To the best of our knowledge, the mesoporous Fe_3O_4@carbon core-shell nanoparticles have not been reported for application in electrode of electrochemical sensor, especially for heavy metal ion.

Herein, a facile one-step hydrothermal approach to synthesize mesoporous Fe_3O_4@carbon core-shell nanospheres was reported. Furthermore, they were modified onto the surface of a magnetic glassy carbon electrode for heavy metal sensors. Owing to the unique porous structure and carbon shell, the Fe_3O_4@carbon core-shell nanospheres electrode delivered significant electrochemical activity and cycling stability.

2. EXPERIMENTAL

2.1 Preparation of Fe_3O_4@carbon core-shell nanospheres

The Fe_3O_4@carbon core-shell nanospheres were prepared by one-step hydrothermal approach according to previous work [19]. In a typical synthesis, ferrocene (0.60g) was dissolved in acetone (60.0mL). After intense sonication for 30.0min, 3.0mL of hydrogen peroxide was slowly added into the above mixture solution, which was then vigorously stirred for 30.0min with magnetic stirring. After that, the precursor solution was transferred to the Teflon-lined stainless autoclave with a total volume of 50.0mL, and then heated to and maintained at 240.0℃. After 18.0h, the autoclave was cooled naturally to room temperature. After intense sonication for 15.0min, the products from the Teflon-lined stainless autoclave were magnetized for 10.0min by a magnet with 0.20T, and the supernatant was discarded under a magnetic field. The precipitates were then washed with acetone three times to remove excess ferrocene. Finally, the black products were dried at room temperature in a vacuum oven.

2.2 Characterization

Raman spectrum was measured on a Jobin-Yvon Lab Ram HR800 Raman spectroscope equipped with a 514.5nm laser source.

Structures of the sample were characterized by a Bruker D8 Avance X-ray diffractometer using Cu Ka radiation at a scan rate of 5^o/min.

IR spectrum was collected on a Bruker TENSOR27 IR spectroscope equipped.

The morphology of sample was investigated by a field emission scanning electron microscope (SEM, Hitachi S-4700).

The morphology of sample was investigated by transmission electron microscope (TEM, JEOL2100).

Superconducting quantum interference device (SQUID) magnetometer (Quantum Design MPMS XL-7) was used to measure the magnetic properties of as-prepared sample

The Brunauer-Emmett-Teller (BET) method was utilized to calculate the specific surface areas using adsorption data in a relative pressure range of 0.05 to 1.0. The pore size distributions (PSD) were derived from the adsorption branch of the isotherms using the Barrett-Joyner-Halenda (BJH) model.

2.3 Electrochemical characterization

The MGCE was polished carefully to a mirror-like finish with 0.05mm alumina slurries and sequentially sonicated for 4.0min in ultrapure water. The electrode was allowed to air-dry. Then 8.0mL 4.0mg/mL of the Fe_3O_4@C suspension was added dropwise on the surface. The Fe_3O_4@C were firmly attached to the MGCE surface due to the magnetic force. The resulting Fe_3O_4@C/MGCE was washed thoroughly with water and stored at 4.0℃ when not in use.

The electrochemical measurements (cyclic voltammetry and electrochemical impedance spectroscopy) were conducted in a 3-electrode single-cell system in the NaAc-HAc electrolyte (pH 5.0). The Fe_3O_4@C/MGCE electrode with 1.0cm×2.0cm, Pt-wire and Ag/AgCl electrodes were used as working, counter and reference electrodes, respectively with CHI1140A electrochemical workstation (CHI110, Austin, TX). All electrochemical measurements were carried out at room temperature. To eliminate the effect of dissolved oxygen, the electrolyte was purged with nitrogen gas for half an hour.

The square wave anodic stripping voltammetry (SWASV) was applied for the electrochemical detection in the NaAc-HAc electrolyte (pH 5.0) containing the target analyte (Pb^{2+}, Hg^{2+} and Cd^{2+}) with various concentration. SWASV responses were recorded with a step potential of 5.0mV, amplitude of 20.0mV, and frequency of 25.0Hz. A desorption potential of 0V for 180.0s was performed to remove the residual metal ions under stirring conditions.

3. RESULTS AND DISCUSSION

Fig.1A showed the X-ray diffraction (XRD) pattern of the as-prepared sample. The reflections peaks at 30.5^o, 36.0^o, 43.6^o, 54.0^o, 57.8^o and 63.0^o were indexed to (220), (311), (400), (422), (511) and

(440) lattice planes of cubic Fe_3O_4 (JCPDS card No. 88-0315), respectively [15]. In addition to this, there was a diffraction peak at around 23.0°, which was ascribed to the (002) plane of amorphous carbon [16]. The size of Fe_3O_4 nanocrystals was calculated to be ca. 9.6nm with Debye-Scherrer formula [17]. Fig.1B showed the FT-IR spectrum of as-prepared sample. The absorption peak at 570.0cm^{-1} was attributed to the Fe-O stretching vibration of Fe_3O_4 [17]. In addition, the peak at around 1652.5 cm^{-1} was assigned to C=C vibration. At the same time, the two peaks at 1699.0cm^{-1} and 3446.0cm^{-1} indicated the existence of carboxyl [18]. Raman spectrum of the as-prepared sample in the range 200.0cm^{-1} to 3000.0cm^{-1} was shown in Fig.1C. The peak at 1585.0cm^{-1} was attributed to the in-plane bond stretching motion of pairs of carbon sp^2 atoms, which also existed as the G mode with the E_{2g} symmetry. The D mode of graphite at 1378.0cm^{-1} was related to the degree of disorder in carbon sp^2 bonded clusters in graphite crystal [20]. These results indicated the formation of Fe_3O_4@C nanospheres.

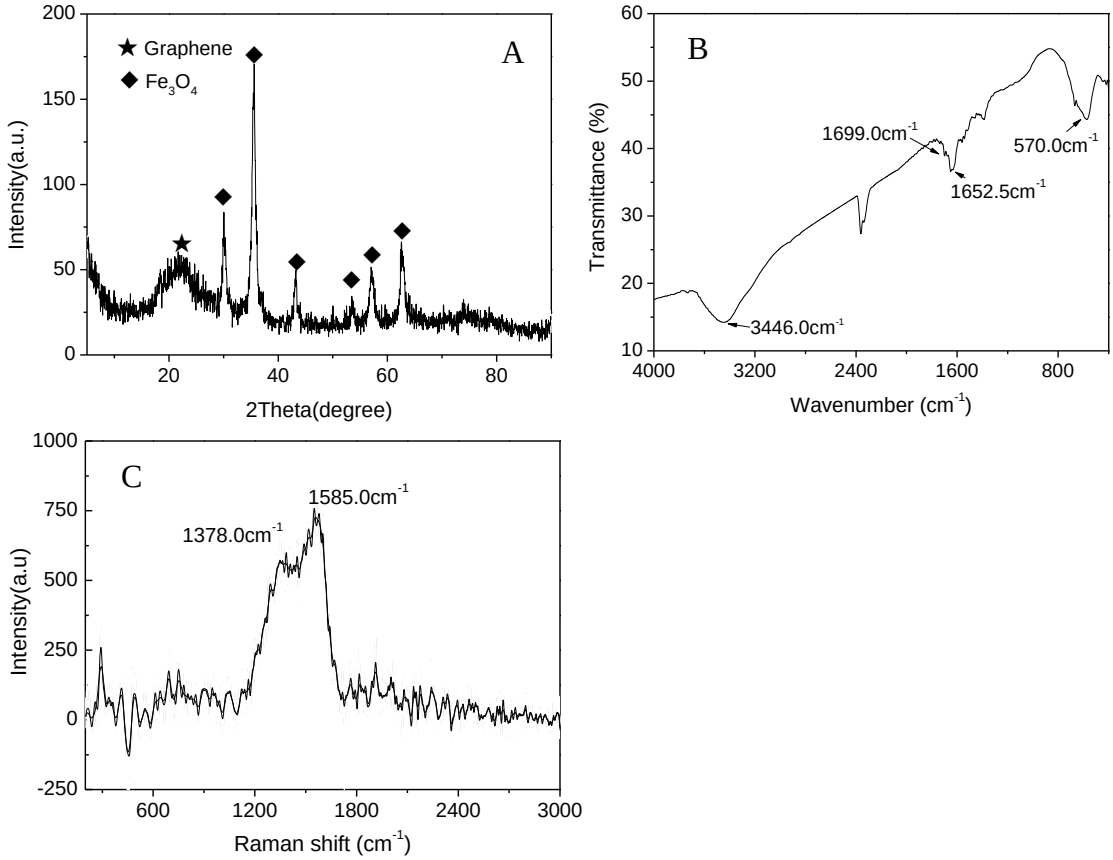

Figure 1. (A) XRD, (B) FT-IR and (C) Raman spectrum of Fe_3O_4@C nanospheres.

The mocrostructure of the Fe_3O_4@C nanospheres was characterized by SEM and TEM image as shown in Fig.2A and Fig.2B, respectively. It could be seen that the Fe_3O_4@C was spherical shape with an average size of ca. 110.0nm. In addition, Fig.2B clearly showed that the Fe_3O_4@C nanosphere has a shell structure with a thickness of 10.0nm which was composed of Fe_3O_4 nanocrystals with a size of about 9.3nm. The size of nanocrystals was almost consistent with the result of XRD. The Fe_3O_4@C

nanospheres were further confirmed by EDS spectrum as shown in Fig.2C. It confirmed the presence of C, Fe and O elemental signatures for the product [17]. The result further confirmed the formation of Fe_3O_4@C nanospheres. At the same time, it also showed the loading amount of Fe_3O_4 in Fe_3O_4/C nanospheres was about 88.5wt%. A typical schematic of our reaction process was illustrated in Fig.2D. In the process of ferrocene decomposition, iron atoms firstly were oxidized into magnetite under the assistance of hydrogen peroxide. The nanocrystals under supersaturated solution would aggregate into larger secondary clusters with increasing in concentration of magnetite. At the same time, the carbon was formed by decomposition from ferrocene, and then adsorbed on the surface of magnetite particles by chemical bonding, leading to the formation core-shell structure [20]. Fig.2D showed the schematic diagram of the Fe_3O_4/C nanosphere' structure. The Fe_3O_4 clusters were encapsulated with carbon shell with porous structure. It provided more channels and active surface area within the composite nanosphere, which allowed metal ions easily penetrating to the inner of composite and thus accelerating the interfacial reaction. Finally, the Fe_3O_4/C nanospheres were adsorbed on surface of the MGCE surface due to the magnetic force and were porous structure for effective against the volume change problem during electrochemical reaction. These characteristics make the porous Fe_3O_4/C nanospheres to act as good electrode of sensor for application in electrochemical detection.

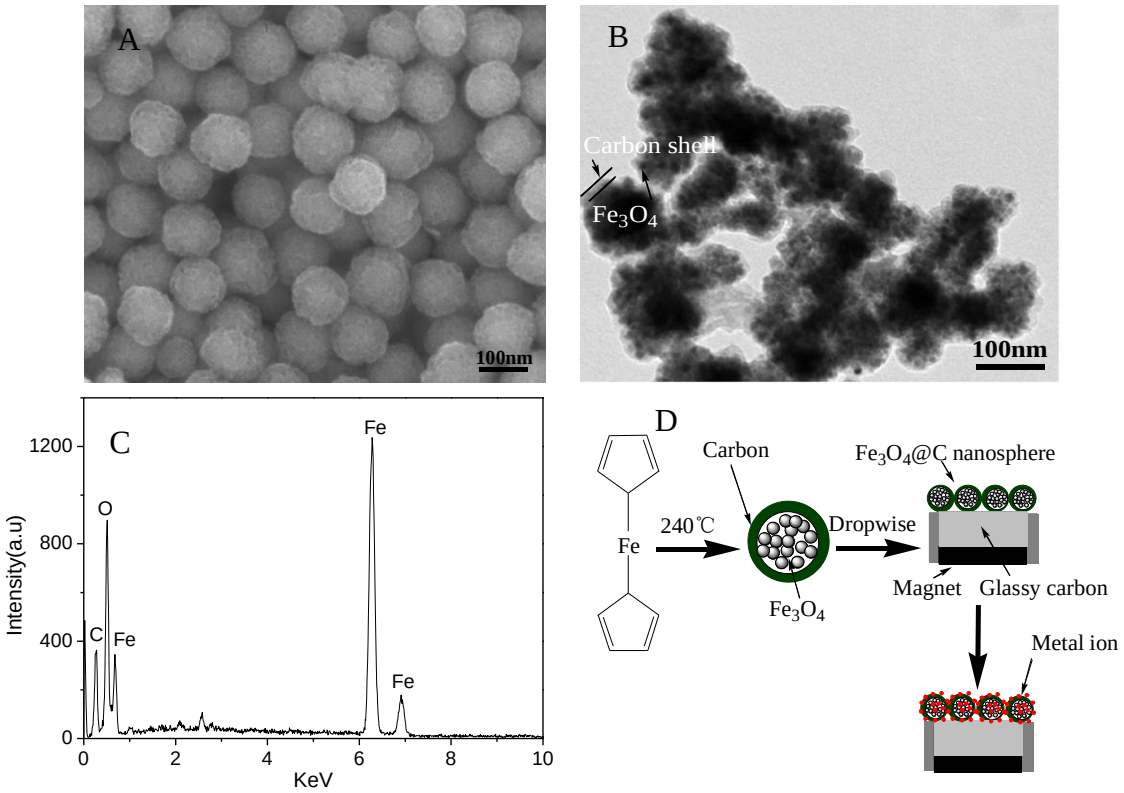

Figure 2. (A) SEM image and (B) TEM image and (C) EDS spectrum of Fe_3O_4@C nanosphere. (D) is schematic diagram of the the synthesis of Fe_3O_4@C nanosphere as an electrode material for determination of metal ions.

Magnetization curve of as-obtained product was shown in Fig.3A. The result indicated that the sample possessed superparamagnetic properties at room temperature due to the negligible coercivity (Hc) and remanence (Mr) in the absence of external magnetic field [21]. The saturation magnetization (*Ms*) of Fe_3O_4@C nanosphere was about 44.4emu/g. When the Fe_3O_4@C nanospheres were dispersed into liquid, they were easily separated entirely from the suspension by an external magnet as shown in the inset of Fig.3A. It was well known that neither the mechanical mixture of Fe_3O_4 particles nor carbon responded to an external magnet, and Fe_3O_4 particles were easily separated from the suspension while the carbon would remain in suspension. The result further confirmed the formation of Fe_3O_4@C nanospheres. Fig.3B represented the N_2 adsorption-isotherms for Fe_3O_4@C nanospheres. The shape of nitrogen isotherms for the product was IV-type curve according the IUPAC classification[18]. This result indicated the Fe_3O_4@C nanosphere with mesopores, in which the size distribution of mesopore was about 2.9nm as showm in Fig.3C.

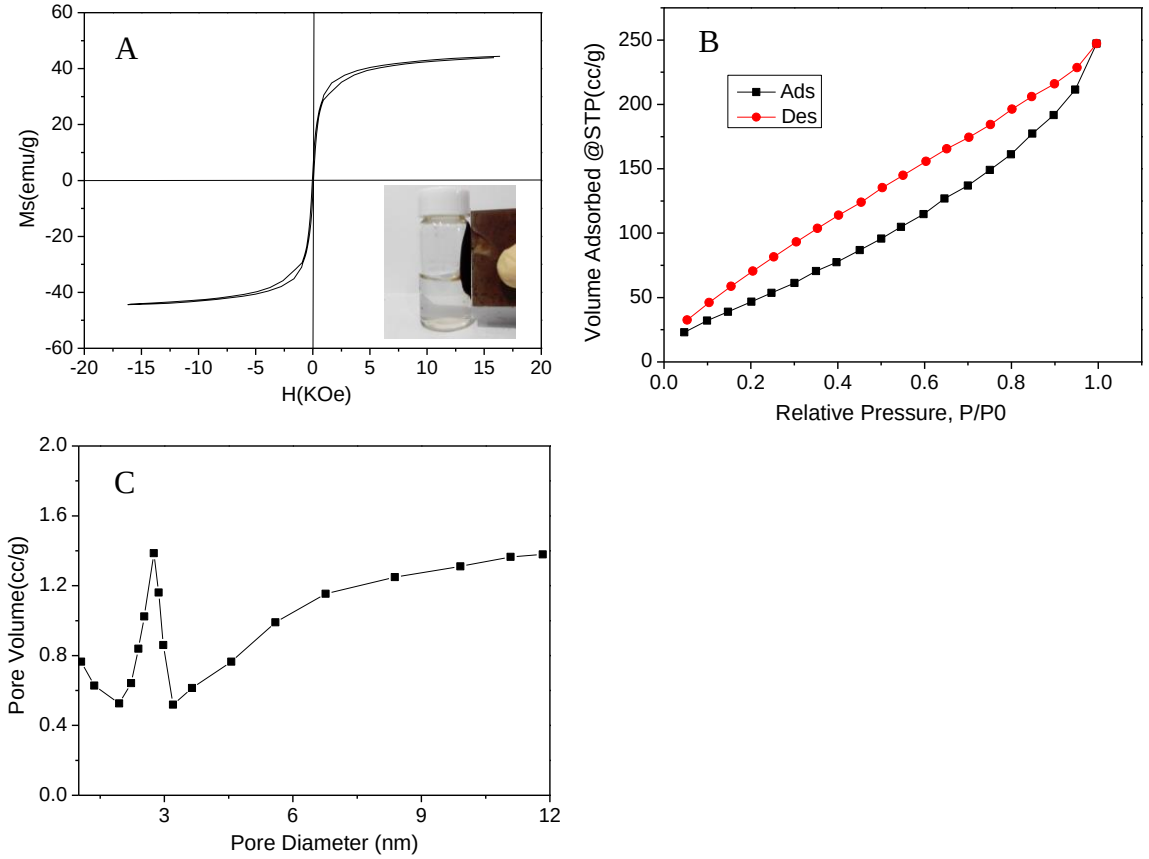

Figure 3. (A) VSM, (B) N_2 isothermal adsorptions and (C) BJH pore distribution of Fe_3O_4@C nanosphere. The inset of Fig.3A is the photograph of Fe_3O_4@C nanosphere in aqueous solution under magnet.

The origin of these mesoporous was attributed to the carbon shell and spaces between particles of the nanometric sizes leading to an inter-particle porosity as shown in Fig.2D. The BET surface area of Fe_3O_4@C nanospheres was about 217.5m^2/g. The high BET surface area of Fe_3O_4/C nanospheres

was attributed to better homogeneous coverage of Fe_3O_4 nanoparticles in carbon shell [22-24]. It was well-known that the surface area was a important parameter for any material to deliver excellent electrochemical performances. The large surface area leaded to the complete participation of the active material during the electrochemical reaction [25]. This unique feature resulted in large surface area and numerous open mesopore channels for electrolyte access and facilitates the ultrafast diffusion of ions during the electrochemical detection, which was very important for improving the sensitivity.

The GNP/GCE was firstly characterized by cyclic voltammograms (CV) and electrochemical impedance spectra (EIS). Compared with the bare GCE, the anodic and cathodic peak currents of the Fe_3O_4@C modified GCE was higher (in Fig.4A). The increase of peak current was contributed to the modified Fe_3O_4@C, indicating that the rate of electron transfer at the Fe_3O_4@C electrode has been increased. In addition to this, it indicated that the Fe_3O_4@C electrode has better electrochemical catalytic behavior and promotion of electron transfer process at the modified electrode surface [15]. The result was attributed to the high activity of the Fe_3O_4@C nanosphere. The interface properties of the modified electrodes using Fe_3O_4@C nanospheres were further confirmed by EIS as shown in Fig.4B. When the Fe_3O_4@C nanospheres were modified onto the GCE, the semicircle diameter of EIS (Rct) was obvious larger comparing with the naked glassy carbon electrode. It indicated that the Fe_3O_4@C coatings provided larger ohmic drop with respect to the naked glassy carbon electrode [15]. Furthermore, the result indicated that the Fe_3O_4@C obstructed electron-transfer between the electrode and the electrochemical probe. These results were consisted with the CV of Fe_3O_4@C electrode.

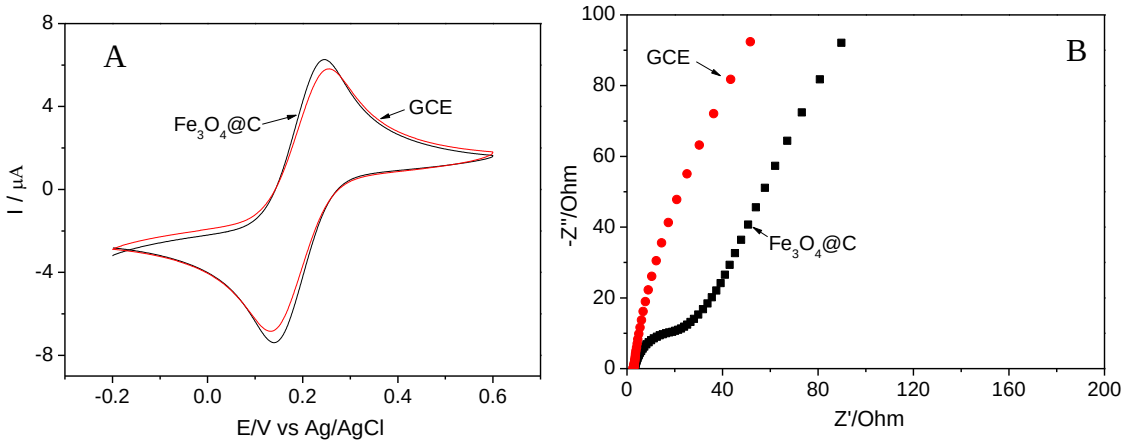

Figure 4. (A) cyclic voltammetric responses and (B) electrochemical impedance spectra of bare GCE and Fe_3O_4@C modified GCE.

Fig.5A showed the SWASV responses of the Fe_3O_4@C electrode toward Pb(II) over the concentration range of 0.1 to 1.5μM in 0.1M NaAc-HAc (pH 5.0). As seen from the calibration plot of Pb(II) (inset in Fig. 5(A)), the peak currents increased linearly versus the Pb(II) concentrations. The sensitivity and limit of detection (LOD) were calculated to be ca.95.6μA/μM and 0.17μM (3σ method), respectively. The results were summarized and compared with the results reported in previous works in Table 1.It demonstrated that the highest sensitivity toward Pb(II) could be obtained on the Fe_3O_4@C modified electrode. Under the optimal experimental conditions, Cd(II) and Hg(II) were also

determined on Fe_3O_4@C modified electrode using SWASV as shown in Fig.5B and5C, respectively. A sensitivity of 7.4μA/μM and 0.91μA/μM with a detection limit of 0.063μM and 0.032 μM (3σ method) were obtained for detection of Cd(II) and Hg(II), respectively. The obtained stripping current toward Pb(II) was around 13 and 105 times higher than that of Cd(II) and Hg(II) as shown in Fig.5D, respectively. The result indicated that Fe_3O_4@C modified electrode showed a high selectivity toward Pb(II). Here, the high sensitivity and selectivity of Fe_3O_4@C electrode toward Pb(II) was attributed to following reasons: (1) the Fe_3O_4@C nanospheres had higher adsorption ability for Pb(II) metal ions, resulting from the high surface negative charges, the coordination between carboxyl groups and Pb(II) metal ion and mesoporous carbon shell; (2) the Fe_3O_4@C nanospheres provided larger active surface area and effective accessible channels for Pb(II) metal ion, resulting from good dispersion of Fe_3O_4 and mesoporous structure of carbon shell.

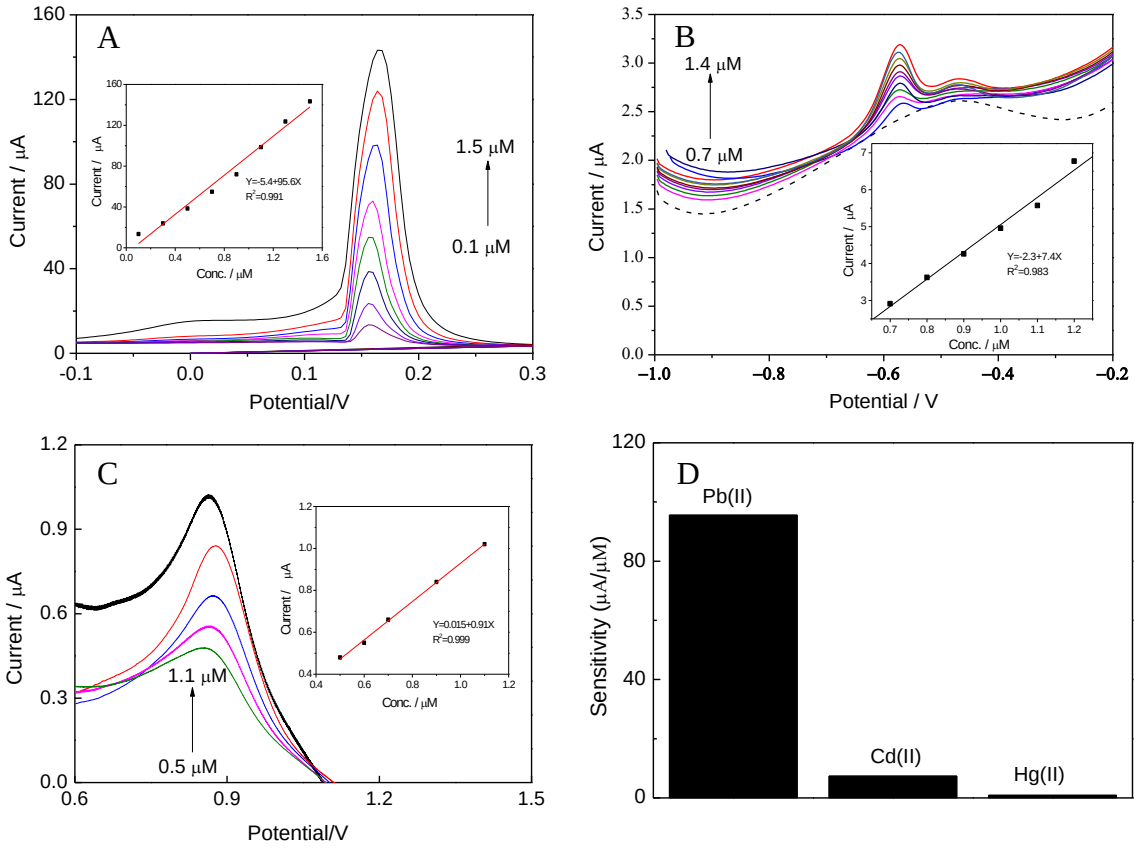

Figure 5. SWASV responses and the corresponding calibration plots of Fe_3O_4@C modified electrode towards (A) Pb(II), (B) Cd(II) and (C) Hg(II) at different concentrations in 0.1M NaAc-HAc solution (pH 5.0).

Therefore, the physical adsorption and chemical adsorption of Fe_3O_4@C electrode both played important roles for the detection of Pb(II) metal ions, which greatly enhanced the sensitivity and selectivity of the colloidal nanoparticles for Pb(II) metal ions.

Table 1. Comparison of current sensitivity with previously reported values of different electrodes for Pb(II) electrochemical sensing.

Electrodes	Sensitivity (μA/μM)	LOD(μM)	Ref.
Fe_3O_4@C GCE	95.6	0.170	This work
Band Fe_3O_4/rGO GCE	13.6	0.169	15
Fe_3O_4/MWCNTs GCE	11.4	6.0pM	14
MnO_2 GCE	22.4	---	26
rGO/MWCNTs GCE	42.1	0.052	27
SnO_2/graphene GCE	18.6	0.0018	28
Porous Co_3O_4 GCE	71.5	0.018	29

The stability of electrode was also very important for practical application in electrochemical detection. Fig.6A showed the cycling performance of the Fe_3O_4@C electrode towards detection of Pb(II) at 0.17 μM, in which the various cycle was stored in air 3 days. It clearly showed that the peak current slightly decreased with increasing in cycling test and became stable after 10 cycling test. The peak current was remained 98.5% of initial peak current after 10 cycles and 30 days. These results indicated that the Fe_3O_4@C electrode exhibited good cycling stability and long-term durability. The EIS of Fe_3O_4@C electrode before and after 10 cycling test was further compared as shown in Fig.6B. There was almost no change in ESR before and after 10 cycling tests, indicating that the effect of cycling test on internal resistance of the Fe_3O_4@C was slight. In addition to this, a slight increase in *R*ct was observed before and after 10 cycling test. This new semi-circle suggested the emergence of a new interface of high resistance during the cycling test. These results demonstrated that the Fe_3O_4@C could be as electrochemical active materials applied in electrochemical detection of Pb(II) metal ions. Based on the above results, the high cycling stability and long-term durability of Fe_3O_4@C electrode towards detection of Pb(II) was attributed to following reasons: (1) the Fe_3O_4/C nanospheres was adsorbed on surface of the MGCE surface due to the magnetic force; (2) the Fe_3O_4/C nanospheres was porous structure for effective against the volume change problem during electrochemical reaction with Pb(II) metal ions.

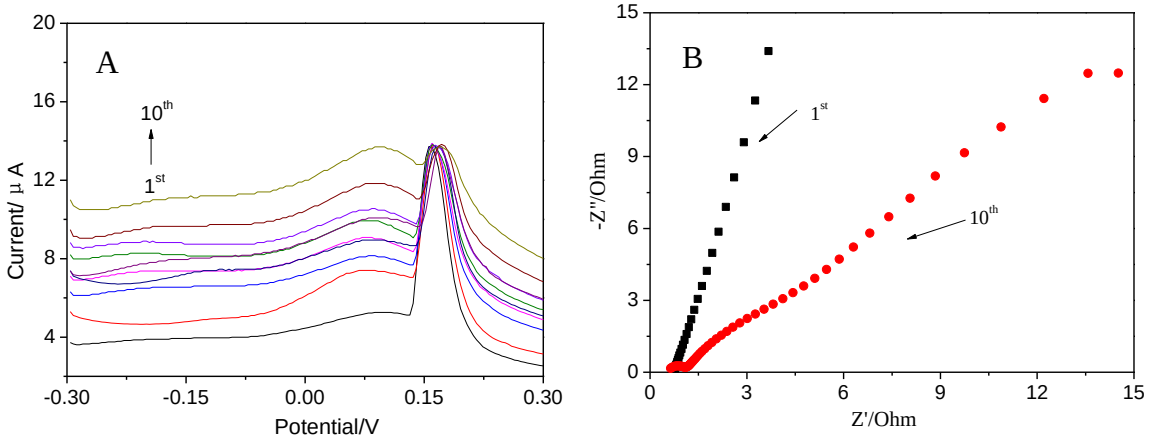

Figure 6. (A) SWASV responses and (B) EIS of Fe_3O_4@C electrode towards Pb(II) from 1st cycle to 10th cycle.

The above results validated that the Fe3O4@C electrode provided a new platform for the detection of Pb(II) in distilled water. To further illustrate the practicality of the Fe3O4@C electrode, real drinking water with and without the addition of Pb(II) were tested. There was no obvious peak current at the SWASV response ofthe real drinking water. This revealed that the concentrations of Pb(II) in the real drinking water was less than 0.17μM and was consistent with the result of the inductively coupled plasma(ICP). The SWASV response of the real drinking water with addition of 0.17μMPb(II) was shown in Fig.7. It clearly showed obvious peak current at the SWASV response of the real drinking water with addition of 0.17μMPb(II). The satisfactory recovery (100.5%) of Pb(II) were obtained by the calibration plots of Fe3O4@C modified electrode in these experiments (in Table 2), which proved that the compositions of real water samples could not influence the sensing of Pb(II) remarkably. The result indicated the potential application of our sensors for the analysis of real samples.

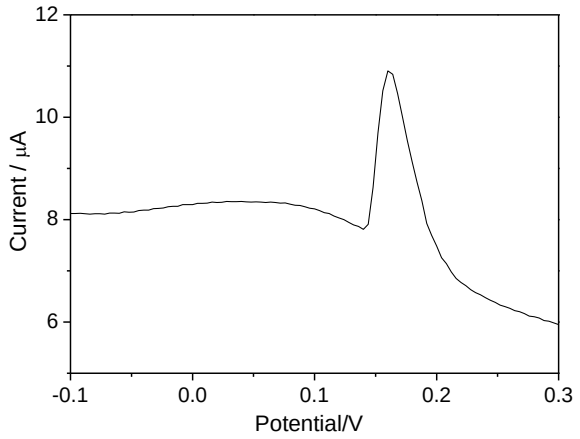

Figure 7. SWASV response of Fe_3O_4@C modified electrode in the real drinking water with addition of 0.17μMPb(II).

Table 2. Analytical results of Pb(II) in real water samples

Sample	Added(μM)	Found(μM)	Recovery(%)
drinking water	0.1700	0.1709	100.5

4. CONCLUSION

In summary, the Fe_3O_4@carbon core-shell nanoparticles was designed and prepared by a facile one-step method. Furthermore, the Fe_3O_4@C nanospheres acted as electrode material on electrochemical detection of Pb(II), Cu(II) and Hg(II) was investigated in detail. The selectivity in individual electrochemical determination of Fe_3O_4@C modified electrode was as follows: Pb(II)>Cd(II)>Hg(II). The line arrange, sensitivity and limit of detection of Fe_3O_4@C electrode towards detection of Pb(II) were about 0.1~18.0μM (correlation coefficient, R_2=0.991), 95.6μA/μM,

and 0.17μM, respectively. Moreover, the electrocatalytic current of the Fe_3O_4@C electrode toward Pb(II) still remained 98.5% and became stable after 10 cycling tests, indicating the excellent cycling stability. These findings showed the applicability of the Fe_3O_4@C electrode as a reliable sensor for detection of Pb(II).

ACKNOWLEDGMENTS
The authors are grateful for the support by the National Natural Science Foundation of China (No. 51622507, 61471255, 61474079, 61501316, 51505324), Doctoral Fund of MOE of China (No. 20131402110013), 863 Program (2015AA042601), Shanxi Province Foundation for Youths (No. 2014021023-3).

References

1. A. A. Gouda, S. M. A. Ghannam. *Food Chem.* 202(2016) 409.
2. A. Chakraborty, S. Bhattacharyya, A. Hazra, A.C. Ghosh, T. K. Maji. *Chem. Commun.* 52(2016) 2831.
3. J. Barton, M. B. G. Garcia, D. H. Santos, P. Fanjul-Bolado, A. Ribotti, M. McCaul, D. Diamond, P. Magni. *Microchim. Aata.* 183(2016) 503.
4. I. Ugulu. *Appl. Spectrosc. Rev.* 50(2015), 113.
5. L. N. Neupane, E. T. Oh, H. J. Park, K. H. Lee. *Anal. Chem.* 88(2016) 3333.
6. S. M. Choi, D. M. Kim, O. S. Jung, Y. B. Shim. *Anal. Chim. Acta*. 892(2015) 77.
7. M. B. Gumpua, S. Sethuraman, U. M. Krishnan, J. B. B. Rayappana. *Sensors. Actuat. B-Chem.* 213(2015) 515.
8. H. L. Fan, S. F. Zhou, J. Gao, Y. Z. Liu. *J. Alloy. Compd.* 671(2016) 354.
9. N. N. Li, T. F. Kang, J. J. Zhang, L .P. Lu, S. Y. Cheng. *Anal. Methods*. 7(2015) 5053.
10. S. Wu, H. N. Wang, S. Y. Tao, C. Wang, L. H. Zhang, Z. G. Liu, C. G Meng. *Anal. Chim. Acta.* 686(2011) 81.
11. Y. Zhang, P. Chen, F. F. Wen, B. Yuan, H. G. Wang. *J. Electroanal. Chem.* 761(2016) 14.
12. C. Gao, X.Y. Yu, S.Q. Xiong, J.H. Liu, X.J. Huang. *Anal. Chem.* 85(2013) 2673.
13. J. Wei, S. S. Li, Z. Guo, X. Chen, J. H. Liu, X. J. Huang. *Anal. Chem*. 88(2016) 1154.
14. Y. L. Yang, Y. You, Y. C. Liu, Z. S. Yang. *Microchim. Acta*. 180(2013) 379.
15. Y.Y. Sun, W.H. Zhang, H.L. Yu, C.L. Hou, D.S. Li, Y.H. Zhang, Y.Q. Liu. *J. Alloy. Compd*. 638(2015) 182.
16. Z H. Zhang, F. Wang, Q. An, W. Li, P.Y Wu. *J. Mater. Chem. A*, 3(2015) 7036.
17. J. Pu, L. Shen, S.Y. Zhu, J. Wang, W. Zhang, Z.H. Wang. *J. Solid. State. Electr.*, 18(2014) 1067.
18. J. Liu, Y.C. Zhou, F. Liu, C.P. Liu, J.B. Wang, Y. Pan, D. F. Xue. *RSC. Adv*. 2(2012) 2262.
19. H. Wang, Y.B. Sun, Q.W. Chen, Y.F. Yu, K. Cheng. *Dalton T.*, 39(2010) 9565.
20. R. Prakash, K. Fanselau, S.H. Ren, T.K. Mandal, C. Kübel, H. Hahn, M. Fichtner. *Beilstein J. Nanotechnol.* 4(2013) 699.
21. Y. Y. Sun, Q. Liang, Y. J. Zhang, Y. Tian, Y.Q. Liu, F.X. Li, D.N. Fang. *J. Magn. Magn. Mater.* 332(2013) 85.
22. M. T. Tran, T. H. T. Nguyen, Q. T. Vu, M. V. Nguyen. *Front. Mater. Sci.* 10(2016) 56.
23. S. Challagulla, R. Nagarjuna, Ra. Ganesan, S. Roy. *ACS Sustainable Chem. Eng.* 4(2016), 974.
24. M. Abdollahi-Alibeik, A. Rezaeipoor-Anari. *J. Magn. Mgan. Mater.* 398(2016) 205.
25. A .L. Tomas-Garcia, Q. F. Li, J. O. Jensen, N. J. Bjerrum. *Int. J. Electrochem. Sci.* 9(2014) 1016.
26. Q. X. Zhang, H. Wen, D. Peng, Q. Fu, X. J. Huan. *J. Electroanal. Chem*. 739(2015) 89.
27. J. T. Zhang, Z. Y. Jin, W. C. Li, W. Dong, A. H. Lu. *J. Mater. Chem. A.* 1(2013), 13139.

28. Y. Wei, C. Gao, F. L. Meng, H. H. Li, L. Wang, J. H. Liu, X. J. Huang. *J. Phys. Chem. C.* 116(2012) 1034.
29. Z. G. Liu, X. Chen, J. H. Liu, X. J. Huang. *Electrochem. Commun.* 30(2013) 59.